Environ Geochem Health (2024) 46:357
https://doi.org/10.1007/s10653-024-02137-6

ORIGINAL PAPER

Synthesis of bis(2-aminoethyl)amine functionalized mesoporous silica (SBA-15) adsorbent for selective adsorption of Pb^{2+} ions from wastewater

Kokila Thirupathi · Madhappan Santhamoorthy · Ranganathan Suresh · Mohammad Ahmad Wadaan · Mei-Ching Lin · Seong-Cheol Kim · Keerthika Kumarasamy · Thi Tuong Vy Phan

Received: 27 May 2024 / Accepted: 16 July 2024 / Published online: 31 July 2024

Abstract Rapid growth in the industry has released large quantities of contaminants, particularly metal discharges into the environment. Heavy metal poisoning in water bodies has become a major problem due to its toxicity to living organisms. In this study, we developed a 3-chloropropyl triethoxysilane incorporated mesoporous silica nanoparticle (SBA-15) based adsorbent utilizing the sol–gel process and Pluronic 123 (P123) as a structure-directing surfactant. Furthermore, the produced SBA-15 NPs were functionalized with bis(2-aminoethyl)amine (BDA) using the surface grafting approach. The physical and chemical properties of the prepared SBA-15@BDA NPs were determined using a variety of instruments, including small-angle X-ray diffraction (SAXS), Fourier-transform infrared (FTIR), scanning electron microscope (SEM), N_2 adsorption–desorption, thermogravimetric, particle size distribution, and zeta potential analysis. The MSN has a large surface area of up to 574 m^2/g, a pore volume of 0.57 cm^3/g, and a well-ordered mesoporous nanostructure with an average pore size of 3.6 nm. The produced SBA-15@BDA NPs were used to adsorb selectively to lead (Pd^{2+}) ions from an aqueous solution. The adsorption study was performed under various conditions, including the influence of solution pH, adsorbent dose,

Kokila Thirupathi, Madhappan Santhamoorthy, Ranganathan Suresh have contributed equally to this work.

K. Thirupathi
Department of Physics, Government Arts and Science College for Women, Karimangalam, Dharmapuri, Tamil Nadu 635111, India

M. Santhamoorthy
School of Chemical Engineering, Yeungnam University, Gyeongsan 38541, Gyeongbuk, Republic of Korea

M. Santhamoorthy · S.-C. Kim
Department of Physiology, Saveetha Dental College and Hospitals, Saveetha Institute of Medical and Technical Science (SIMATS), Saveetha University, Chennai 600077, India

R. Suresh
Department of Chemistry, Centre for Material Chemistry, Karpagam Academy of Higher Education, Coimbatore, Tamil Nadu 641021, India

M. A. Wadaan
Department of Zoology, College of Science, King Saud University, P.O. Box 2455, Riyadh 11451, Saudi Arabia

M.-C. Lin · K. Kumarasamy (✉)
Department of Applied Chemistry, Chaoyang University of Technology, Taichung 413310, Taiwan, R.O.C.
e-mail: t5180677@cyut.edu.tw

T. T. V. Phan (✉)
Center for Advanced Chemistry, Institute of Research and Development, Duy Tan University, 03 Quang Trung, Hai Chau, Danang 550000, Vietnam
e-mail: phanttuongvy4@duytan.edu.vn

T. T. V. Phan
Faculty of Environmental and Chemical Engineering, Duy Tan University, 03 Quang Trung, Hai Chau, Danang 550000, Vietnam

adsorption kinetics, adsorption selectivity in the presence of competing metal ions, and reusability. The results of the kinetic study demonstrated that SBA-15@BDA NPs absorb selectively Pb^{2+} ions via chemisorption. The SBA-15@BDA NPs show Pb^{2+} ions with a maximum adsorption capacity of ~88% and an adsorbed quantity of approximately ~112 mg/g from the studied aqueous solution. The adsorption mechanism relies on coordination bonding between Pb^{2+} ions and surface-functionalized amine groups on SBA-15@BDA NPs. Furthermore, the proposed SBA-15@BDA NPs adsorbent demonstrated excellent reusability over five cycles without significantly reducing adsorption performance. As a consequence, SBA-15@BDA NPs might serve as an effective adsorbent for the selective removal of Pb^{2+} ions from aqueous effluent.

Keywords Mesoporous silica adsorbent · Surface functionalization · Metal adsorption · Kinetic study · Recyclability

Introduction

Water contamination is a global concern that affects the lives of millions of people worldwide. It is a major global risk factor for infections, diseases, and deaths, while also reducing the amount of clean drinking water available worldwide (Ashbolt, 2004). Heavy metal poisoning of water resources has long been a serious environmental issue (Plessis, 2022), as they are toxic and carcinogenic contaminants that may accumulate in organisms and infiltrate the food chain (Briffa et al., 2020; Parambadath et al., 2011). Toxic heavy metals such as cadmium (Cd), arsenic (As), lead (Pb), mercury (Hg), chromium (Cr), zinc (Zn), copper (Cu), and nickel (Ni) have been identified as the primary contaminants in water reservoirs (Angon et al., 2024; Moorthy et al., 2013a; Nagappan et al., 2013; Zhang et al., 2023). Such pollutants can disturb the enzymatic systems of people and animals, jeopardizing their health.

Lead (Pb) is one of the most poisonous metals, with harmful effects on both the environment and humans. Lead ion (Pb^{2+}) is discharged into the environment directly or indirectly through industrial wastewater from mining, metallurgical industries, batteries and stabilizers, and alloys (Harikrishnan et al., 2024; Moorthy et al., 2013b; Raj & Das, 2023; Reddy et al., 2023). The accumulation of Pb^{2+} ions in the human body, particularly in the kidneys, may cause organ dysfunction. Lead poisoning can also destroy red blood cells and testicular tissue, as well as lung illness and excessive blood pressure (Bhasin et al., 2023; Moorthy et al., 2013c). Because of the significant consequences of lead contamination, the World Health Organization has established 0.005 mg/L as the acceptable lead content in drinking water. One of the most essential measurements in water purification is to develop an effective process for removing lead ions from the aqueous medium to avoid detrimental effects on the environment and ecological system (Mitra et al., 2022).

There are several techniques were adopted for the removal of heavy metal ions including adsorption, reverse osmosis, solvent-based extraction, membrane processes, ion exchange, evaporation, and chemical precipitation are popular techniques for removing heavy metals like cadmium from polluted water (Aziz et al., 2023; Collin et al., 2022; Moorthy et al., 2013d). Most of these methods are inefficient and produce a large volume of sludge. Among various techniques, the adsorption process is widely employed due to its simplicity, adaptability, cost-effectiveness, insensitivity to contaminants, absence of dangerous chemical production, and capacity to be recycled for reuse (Kumar et al., 2023; Singh et al., 2024).

Solid-phase extraction, which is based on the retention of analytes on solid sorbents, is a particularly successful preconcentration approach due to its rapid adsorption, simplicity, and productivity, as well as its high preconcentration factor (Moorthy et al., 2018; Tahreen et al., 2020; Taslima et al., 2022). In the recent decade, different solid sorbents such as activated carbon (Venugopal et al., 2023), porous and/or functional polymers (Fu & Wang, 2011), and modified silica gels (Moorthy et al., 2013e; Santhamoorthy et al., 2023a) have been developed for the preconcentration and/or adsorption of metal ions and/or organics. The sorbents have desired features such as ease of regeneration and quick, quantitative adsorption.

Among the range of solid-state adsorbent materials, mesoporous silica-based adsorbent materials are considered effective adsorbent because of their excellent physicochemical characteristics

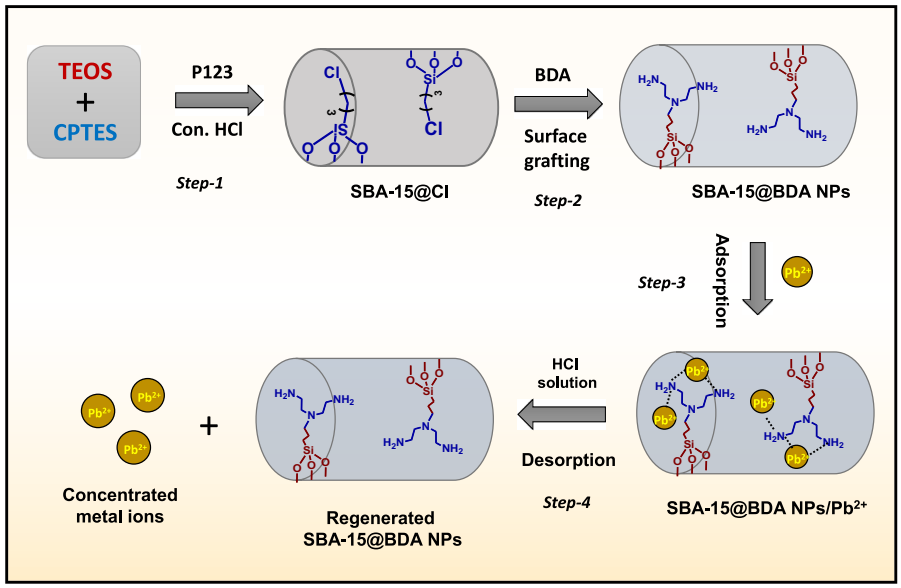

Scheme 1 Represents the synthesis, surface modification, and metal adsorption of SBA-15@BDA NPs

such as highly ordered pore structures and uniform pore sizes (Moorthy et al., 2017a). Two-dimensional (2D) hexagonal Santa Barbara Amorphous (SBA-15) is a mesoporous silica with a controllable pore size and high specific surface area (Moorthy et al., 2016a). Because of its high adsorption ability, SBA-15 may be employed to adsorb heavy metal ions. According to reported studies, organic-functionalized silica nanoparticles surpass unmodified mesoporous molecular sieves in terms of adsorption. Because the surface-modified functional groups can interact with specific metal ions with respect to the nature of ligand groups and the complexing metal ions. Thus, the selectivity of the absorbent materials could be tunable by grafting the surface of the adsorbents using the desired ligand functionalities. Meanwhile, amine-functionalized materials have been shown to have a greater adsorption capacity than unmodified silica nanoparticles (Bharathiraja et al., 2016; Liosis et al., 2021). Because the functional group modifications ($–NH_2$ or –SH moieties) allow these groups to form complexes with specific heavy metal ions (Bharathiraja et al., 2017; Liu et al., 2022). The amine-modified SBA-15 has considerably enhanced adsorption affinity and recyclability because the $–NH_2$ modification improves bonding strength with Pb^{2+} ions (Petrovic et al., 2022).

In this work, 3-chloropropyl triethoxysilane incorporated mesoporous silica (SBA-15) has been synthesized utilizing the sol–gel process based on acidic hydrolysis. The bis(2-aminoethyl)amine (BDA) was then functionalized on the surface of the SBA-15 nanoparticles using a post-surface modification method. The BDA-functionalized SBA-15 (SBA-15@BDA NPs) was described utilizing a variety of instrumental characterizations. Furthermore, the metal ion adsorption efficiency of the produced SBA-15@BDA NPs was determined utilizing a variety of metal ions, including divalent metal ions (Pb^{2+}, Ni^{2+}, Co^{2+}, Cd^{2+}, Zn^{2+} ions) and common metal ions (Na^{+}, K^{+}, Ca^{2+}, and Mg^{2+}). Furthermore, the adsorption properties were investigated under various conditions, such as the influence of solution pH, adsorbent dose, contact duration, and metal ion combination. Furthermore, kinetic investigations were carried out to investigate the adsorption mechanism of SBA-15@BDA NPs towards the specified metal ions in an aqueous solution.

Experimental

Reagents

3-chloropropyl triethoxysilane (CPTES, 95%), tetraethylorthosilicate (TEOS, 98%), polyethylene oxide-polypropylene oxide-polyethylene oxide (P123, 97%), bis(2-diaminoethyl)amine (BDA,

98%), ethanol (99%), hydrochloric acid (HCl, 36%), and metal nitrate salts were purchased from Sigma Aldrich Chemicals (USA). All the reagents were used as received without further purification. The metal ion stock solutions were prepared by dissolving the appropriate metal salt in deionized water and stored at 4 °C. The initial metal ion concentration of the stock solution was prepared with 1 g/L and the appropriate dilutions were performed for the further experimental study.

Preparation of SBA-15 NPs

The synthesis of SBA-15 NPs and its surface modification was performed following the reported literature with slight modifications (Manivasagan et al., 2017a). The mesoporous silica (SBA-15) was prepared utilizing Pluronic P123 as a structure-directing agent using tetraethyl orthosilicate and CPTES (80:20 wt/wt%) mixture as a silica source. Pluronic surfactant was dissolved in 45 mL deionized water containing 3 g HCl under magnetic stirring at 40 °C for 30 min.

After generating a homogenous solution, TEOS (1.5 mL) was slowly added to the surfactant medium while vigorously stirring and further the reaction suspension was allowed for 24 h at 45 °C. Consequently, the obtained white suspension was allowed to crystallize under static hydrothermal conditions at 90 °C. The crystalline product was filtered, washed with water, and dried at 60 °C (Moorthy et al., 2013f, 2016b). The occluded surfactant was removed by the solvent extraction process by treating the powder sample with acidified ethanol and ammonium chloride (Scheme 1, Step-1).

Surface immobilization of BDA onto SBA-15 NPs

About 1 g of extracted SBA-15 material was homogenized in ethanol (50 mL). To this, about 1 mL of bis(2-aminoethyl)amine was added, and the resulting suspension was stirred at 70 °C for 24 h in the presence of triethylamine. After the reaction was completed, the product was filtered, washed with ethanol, and dried at 60 °C (Du et al., 2023; Moorthy et al., 2017b). The obtained sample was labeled SBA-15@BDA NPs (Scheme 1, Step-2).

Characterization

The surface modified functional groups were determined by Fourier transform infrared (FTIR) spectroscopy (Thermo Nicolet 360 instrument). Small-angle X-ray scattering (SAXS) measurements were performed at Pohang Accelerator Laboratory (PAL, Pohang, Korea, 4–16 keV; CoK radiation = 1.608). The organic functional group content in the sample was determined using thermogravimetric analysis (TGA, NETZSCHSTA 409 TG–DTA, Germany). N_2 adsorption–desorption analysis was performed using a Micromeritcs Tristar 3000 analyzer at 77 K. Specific surface areas were calculated using the Brunauer–Emmett–Teller (BET) method. Pore volumes and pore size distributions were determined from the adsorption branches of isotherms using the Barrett–Joyner–Halenda (BJH) model. The particle size distribution and surface charge of the nanoparticles were determined using the zeta potential analyzer (Malvern, Zetasizer). An inductively coupled plasma optical emission spectroscopy (ICP-OES) was used to determine the metal ion concentration in the aqueous solutions.

Adsorption experiments

For the metal ion adsorption experiments, SBA-15@BDA NPs were used as adsorbent. All the metal ion stock solutions were prepared by dissolving appropriate metal salts in deionized water with a solution concentration of 1000 mg/L. To evaluate the adsorption performance of SBA-15@BDA NPs towards Pb^{2+} ion solution, the various factors including solution pH, contact time, and the selective adsorption in the presence of competitive metal ions, and adsorbent dosage, respectively, and recyclability, were determined using 0.1 g of SBA-15@BDA NPs adsorbent in 10 mL of metal ion solution (100 mg/L) (Scheme 1, Step-3).

pH effect

For the experiment, approximately 0.1 g of SBA-15@BDA NPs were used and the volume of Pb^{2+} ion solution was 10 mL (100 mg/mL). The solution pH value was adjusted to 3, 5, 6.5, 7.5 and 9.0. The

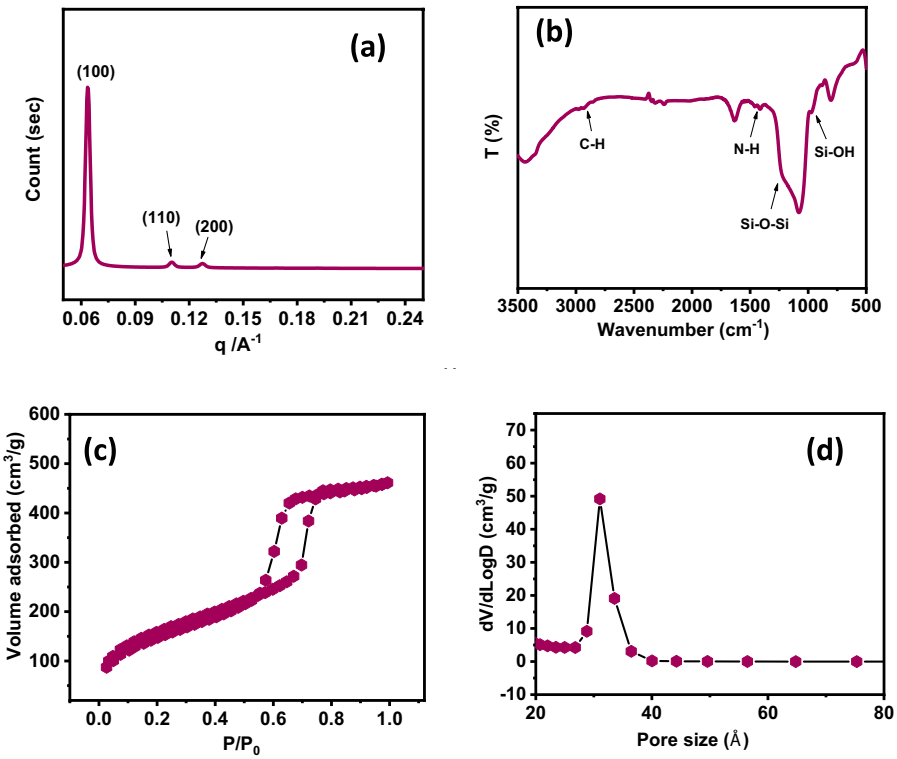

Fig. 1 **a** SAXS pattern, **b** FTIR spectrum, **c** N_2 adsorption–desorption, and **d** pore size distribution analysis of SBA-15@BDA NPs, respectively

adsorbent suspension was shaken at 150 rpm at 25 °C. The reaction contact time was 60 min.

Adsorption kinetics

To carry out this study, approximately 0.1 g of SBA-15@BDA NPs were suspended in the Pb^{2+} ion solution (10 mL, 100 mg/L). The adsorbent suspension was shaken at 150 rpm at 25 °C. About 10 mL of Pb^{2+} ion solution was sampled every specific time. The Pb^{2+} ion concentrations were estimated by ICP–OES spectrometry. Removal efficiency (R_e) and adsorption capacities (q_e, mg/g^{-1}) were calculated by the following equation.

$$\text{Removal efficiency } (\%) = \frac{C_0 - C_e}{C_0} \times 100 \quad (1)$$

$$\text{Adsorption capacity } \left(q_e\right) = \frac{C_0 - C_e}{m} \times V \quad (2)$$

where C_0: initial metal ion concentration; C_e: equilibrium metal ion concentration; V: volume of the solution; m: adsorbent weight.

The kinetic study on the Pb^{2+} ion adsorption was performed by using the pseudo-first-order and pseudo-second-order models. Furthermore, the Langmuir and Freundlich models were adopted to determine the adsorption isotherm models. The adsorption efficiency of the SBA-15@BDA NPs was determined using various concentrations of metal ions. For the kinetics experiment, SBA-15@BDA NPs (0.1 g) were immersed in the different concentrations of Pb^{2+} ion solution (10, 20, 50, 75, 100, and 150 mg/L), respectively. The solution pH was adjusted using HCl or NaOH solution. The selective adsorption efficiency of the SBA-15@BDA NPs was determined in the presence of other competing metal ions. All the other experimental conditions were similar to the kinetic experiments. ICP-AES was used to determine the equilibrium concentration of metal ions. The selective adsorption of Pb^{2+} ions on SBA-15@BDA NPs was depicted in Scheme 1.

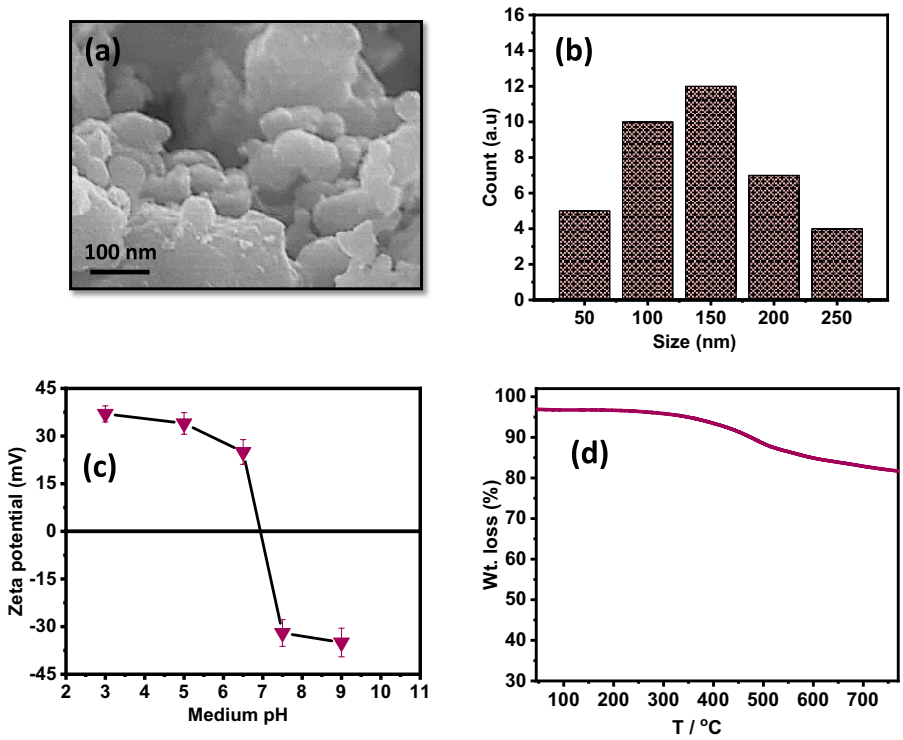

Fig. 2 **a** SEM, **b** Particle size, **c** zeta potential, and **d** TG analysis of SBA-15@BDA NPs

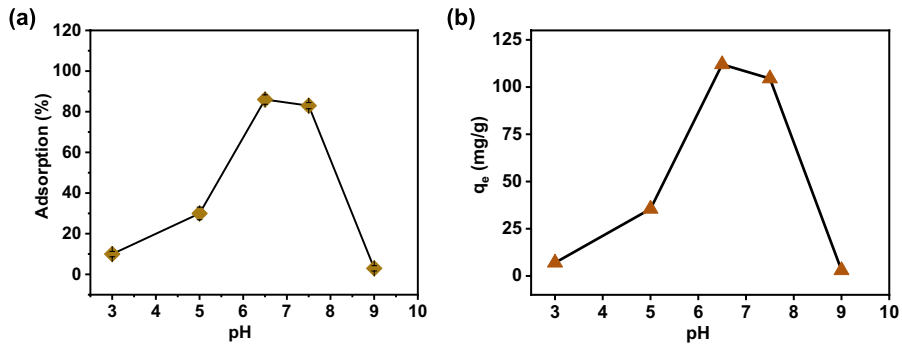

Fig. 3 Effect of pH on the **a** adsorption percentage and **b** adsorption amount of Pb^{2+} ions, on SBA-15@BDA NPs. Initial metal ions concentration: 100 mg/L, adsorbent dose: 0.1 g, shaking rate: 150 rpm, 25 °C

Adsorption–desorption study

The recyclability of the adsorbent is considered an important factor in determining its efficiency. Therefore, the recyclable capacity of the SBA-15@BDA NPs was examined using a sequence of adsorption–desorption experiments. To perform this experiment, Pb^{2+} ion adsorbed SBA-15@BDA NPs (0.1 g) were treated with HCl solution (0.1 M) to remove the adsorbed Pb^{2+} ions. The acid-treated SBA-15@BDA NPs adsorbent was then washed with deionized water and dried at 60 °C. Next, the regenerated adsorbent was utilized for the subsequent adsorption cycle.

Results and discussion

Characterization of the SBA-15@BDA NPs

The formation of ordered mesoporous structured material was verified using SAXS analysis. As shown in Fig. 1a, the SAXS pattern of the BDA functionalized SBA-15@BDA NPs had three scattering peaks (100), (110), and (200) reflections confirming the formation of a well-ordered mesoporous structure material. The peak intensity of (100) is well-resolved in the SBA-15@BDA NPs, confirming that the mesostructured order is retained during the surface grafting

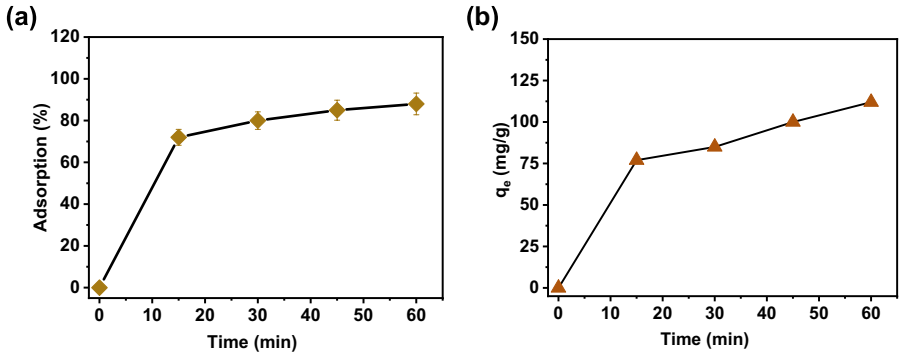

Fig. 4 Effect of contact time on the **a** adsorption percentage and **b** adsorption amount of Pb^{2+} ions, on SBA-15@BDA NPs. Initial metal ions concentration: 100 mg/L, adsorbent dose: 0.1 g, shaking rate: 150 rpm, 25 °C

process of BDA groups (Oh et al., 2017). This result evidenced that the BDA groups can be modified without blocking the mesopores.

The presence of surface functionalized organic groups in the SBA-15@BDA NPs was determined using FTIR analysis. As observed in Fig. 1b, the FTIR analysis of SBA-15@DBA NPs has prominent stretching peaks at 983 cm^{-1} and 1027 cm^{-1} indicating the stretching vibrations of Si–O-Si and Si–OH groups. Furthermore, the SBA-15@BDA NPs exhibited the typical C–H peaks at 2890 cm^{-1}, and 2920 cm^{-1}, which represent the C–H stretching of alkyl carbon groups. Furthermore, the typical bands at 1492 cm^{-1}, and 1523 cm^{-1}, as well as a broad peak at 2712 cm^{-1}–3170 cm^{-1} assigned to C–N and N–H stretching, evidencing that BDA groups were successfully immobilized onto the surface of the SBA-15@BDA NPs (Manivasagan et al., 2017b; Phan et al., 2018). Figure 1c shows the N_2 adsorption–desorption isotherm curves for the mesoporous structured SBA-15@BDA NPs. As displayed in Fig. 1c, d, the SBA-15@BDA NPs showed a type IV isotherm curve with H1 hysteresis representing the formation of typical mesoporous structured materials. The calculated surface area, pore size, and mesopore volume of the SBA-15@BDA NPs are 574 m^2/g, a pore volume of 0.57 cm^3/g, and a pore size of about 3.6 nm, respectively (Santhamoorthy et al., 2022).

Furthermore, the SEM analysis was carried out to evaluate the particle morphology and particle size. As shown in Fig. 2a, the SEM images showed SBA-15@BDA NPs exhibited a flakes-like particle, with an average particle size of about ~150 nm in size (Fig. 2a). The particle size of the SBA-15@BDA NPs was further estimated using particle size analysis. As displayed in Fig. 2b, the SBA-15@BDA NPs had a

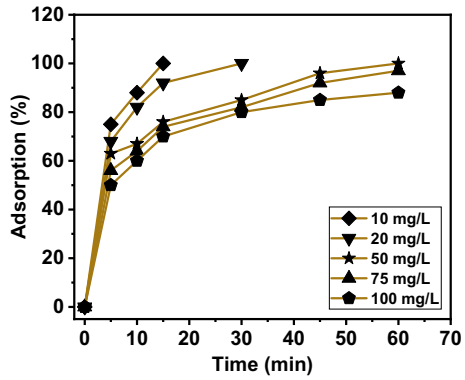

Fig. 5 Effect of adsorption on the SBA-15@BDA NPs from various initial metal ions solution concentrations, respectively. Initial metal ions concentration: 10 -100 mg/L, adsorbent dose: 0.1 g, shaking rate: 150 rpm, 25 °C

particle size in the range between 120 and 450 nm with an average particle size of about ~160 nm. Furthermore, the surface charge of the SBA-15@BDA NPs was determined using zeta potential analysis. As shown in Fig. 2c, the SBA-15@BDA NPs had positive zeta potential values +37 mV, +34 mV, +25 mV at pH 3, 5, 6.5, and negative zeta potential of about −32 mV, −35 mV respectively, at pH 7.5 and 9, representing that the SBA-15@BDA NPs have a high content of amine groups on the surface of the SBA-15@BDA NPs (Thirupathi et al., 2022). The higher content of amine groups becomes protonated under higher acidic pH conditions. Therefore, the SBA-15@BDA NPs showed higher positive charge under reduced pH circumstances. The presence of surface-functionalized organic content in the SBA-15@BDA NPs was determined using TGA analysis. As shown in Fig. 2d, the SBA-15@BDA NPs had a cumulative weight loss of about ~17.5 wt%, in the

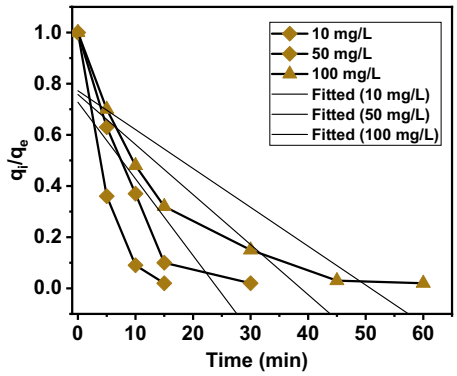

Fig. 6 Adsorption kinetics of the SBA-15@BDA NPs in different concentrations of initial metal ions solutions of Pb^{2+} ions solution. Initial metal ions concentration: 15, 50 and 100 mg/L, adsorbent dose: 0.1 g, shaking rate: 150 rpm, 25 °C

Table 1 The pseudo-second-order rate constant of adsorption kinetics of SBA-15@BDA NPs in aqueous Pb^{2+} ions solutions

Initial conc. of metal ions (mg/L)	K_{ad} (g/mg/min)	R^2
	Pb^{2+}	Pb^{2+}
25	3.8×10^{-3}	0.993
50	5.8×10^{-3}	0.996
100	6.2×10^{-3}	0.981

temperature range between 100 and 650 °C, indicating the thermal decomposition of surface-modified amine functionalities.

Batch adsorption studies

Effect of solution pH

The effect of pH of the adsorption medium was determined at different pH levels, a Pb^{2+} ion solution (10 mL, 100 mg/L) was suspended with SBA-15@BDA NPs, and the medium pH was adjusted appropriately (pH 3, 5, 6.5, 7.5 and 9) at 25 °C. As shown in Fig. 3a, the SBA-15@BDA NPs showed high Pb^{2+} ion adsorption efficiency (~86%) and the adsorption capacity (112 mg/g) when the solution pH was maintained at pH 6.5 (Fig. 3b). Interestingly, the Pb^{2+} ion adsorption was gradually increased from pH 3 to 7 and then the adsorption was decreased considerably when the solution pH was attained to basic pH (pH 8).

Therefore, the adsorption studies were performed at pH 6.5. These results indicate that the competitive adsorption of protons (H^+ ions) and metal ions (Pb^{2+} ions) in the aqueous solution affects the chelation between the functional ligand sites and Pb^{2+} ions. Under reduced pH conditions, the amine groups

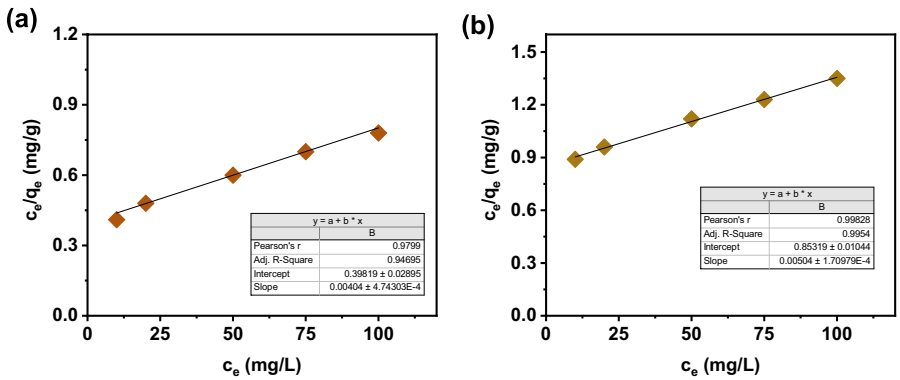

Fig. 7 Equilibrium isotherm of SBA-15@BDA NPs for Pb^{2+} ion adsorption by the **a** Freundlich isotherm and **b** Langmuir models, respectively. Initial metal ions concentration: 10–100 mg/L, adsorbent dose: 0.1 g, shaking rate: 150 rpm, 25 °C

Table 2 Langmuir and Freundlich adsorption isotherm parameters of SBA-15@BDA NPs for Pb^{2+} ions

	Langmuir			Freundlich		
Adsorbent	q_m (mg/g	K_L (L/mg)	R^2	1/n	K_F ((mg/g)/(mg/mL))	R^2
SBA-15@BDA/Pb^{2+}	112	5.9	0.99	1.67	4.2	0.94

become protonates and thus limit the adsorption process (Thirupathi et al., 2023). In contrast, as the pH increased, the protonated amine groups became deprotonate, which in turn, increased the metal ion adsorption at higher pH conditions (Moorthy et al., 2014a). These study results confirmed that the solution pH was a key parameter determining the adsorption efficiency of metal ions.

Effect of contact time

The effect of metal ion adsorption concerning the contact time was studied at different times (0, 15, 30, 45 and 60 min), respectively, with the fixed dosage of SBA-15@BDA NPs (0.1 g) and the Pb^{2+} ions solution (10 mL, 100 mg/L). As shown in Fig. 4, the Pb^{2+} ion adsorption was increased gradually with respect to the contact time.

As observed in Fig. 4a, quick adsorption was attained in the initial 15–30 min, and about ~ 80% of the Pb^{2+} ion adsorption was achieved in 30 min. Adsorption gradually attained equilibrium in 45 min with the maximum adsorption of Pb^{2+} ions at about 86% with the maximum adsorption amount of Pb^{2+} ions estimated to be 112 mg/g (Fig. 4b). The adsorption capacity of the SBA-15@BDA NPs was determined by the content of surface functionalized organic ligand groups, which are responsible for removal of metal ions from aqueous solution (Moorthy et al., 2014b).

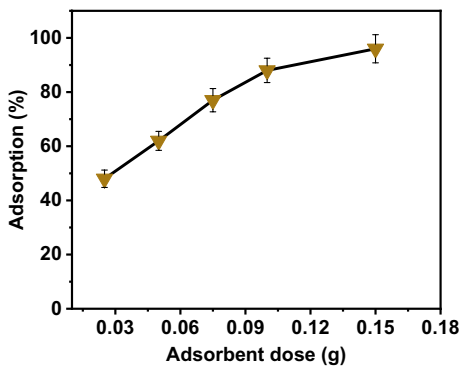

Fig. 8 Dose-dependent adsorption behavior SBA-15@BDA NPs on Pb^{2+} ions. Initial metal ions concentration: 100 mg/L, adsorbent dose: 0.025, 0.05, 0.075, 0.1, and 0.15, shaking rate: 150 rpm, 25 °C

Effect of initial metal ion concentration

SBA-15@BDA NPs' adsorption efficiency was assessed using Pb^{2+} ion solutions at various starting metal ion concentrations (10, 20, 50, 75, and 100 mg/L). As shown in Fig. 5, SBA-15@BDA NPs (0.1 g) showed improved Pb^{2+} ion adsorption capabilities when the starting Pb^{2+} ion solution concentration in the adsorption medium was low (10, 20, and 50 mg/L, respectively). Because of their enhanced amine groups, SBA-15@BDA NPs effectively adsorb Pb^{2+} ions from solutions containing 10–50 mg/L (Fig. 5). On the other hand, when the initial metal ion concentration was increased to 75 and 100 mg/L, the adsorption capacity of the SBA-15@BDA NPs was somewhat reduced. This may be explained by the higher concentration of Pb^{2+} ions in the original solution. As can be observed in Fig. 5, from the starting metal ion concentrations of 10, 20, and 50 mg/L, respectively, the SBA-15@BDA NPs adsorb about 100%, 95%, and 90% of Pb^{2+} ions. When Pb^{2+} ion concentrations start off higher than 100 mg/L, the adsorption trend reaches equilibrium. SBA-15@BDA NPs (0.1 g) effectively eliminated around 86% of Pb^{2+} ions from a solution with low concentration (Park et al., 2014). Because the adsorbent and

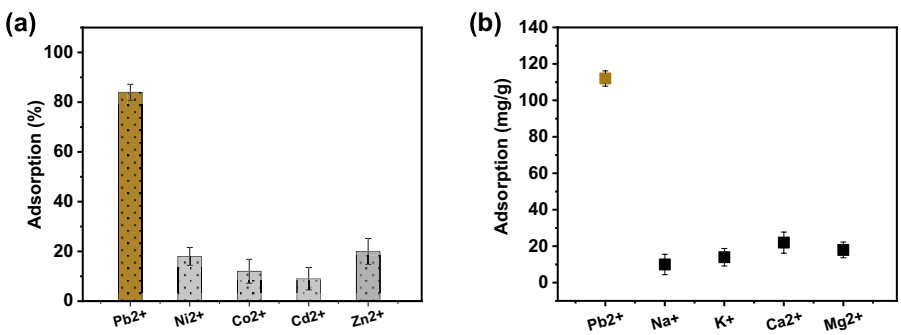

Fig. 9 Selective adsorption of Pb^{2+} ions from **a** heavy metal ions, and b common cations, respectively

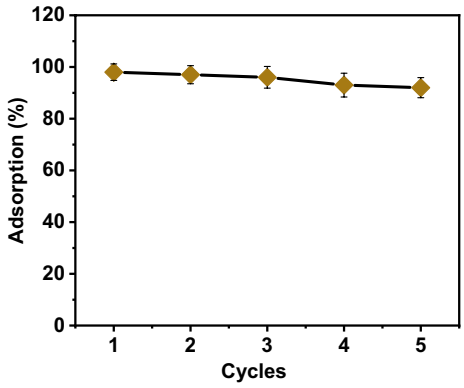

Fig. 10 Recyclable efficiency of the SBA-15@BDA NPs under repeated adsorption–desorption process. Initial metal ions concentration: 100 mg/L, adsorbent dose: 0.1 g, shaking rate: 150 rpm, 25 °C

adsorbate interact differently, the SBA-15@BDA NPs showed varying adsorption capacities towards Pb^{2+} ions.

Consequently, the pseudo-first-order and pseudo-second-order models were used to calculate the adsorption kinetics of Pb^{2+} ions, respectively, using the following equations.

$$dq/dt = \log qe - \frac{k1}{2.303}t \quad (3)$$

$$t/q_t = 1/k_2 q_e^2 + t/q_e \quad (4)$$

where q_e (mg/g) and q_t (mg/g): equilibrium adsorption dosage and equilibrium adsorption capacity at random time t (min), respectively. k_1 (min^{-1}), k_2 (g/mg/min): the adsorption rate constant of the two models, respectively.

The adsorption kinetic data were fitted to Eqs. 1 and 2 and shown in Fig. 6. In addition, Table 1 lists the determined kinetic parameters. The pseudo-second-order model has a higher correlation coefficient (R^2) value for Pb^{2+} ions (0.992) compared to the pseudo-first-order model. The experimental data demonstrated that the adsorption process closely resembles the pseudo-second-order model, implying that the adsorption of Pb^{2+} ions on the SBA-15@BDA NPs surface may constitute a rate-limiting phase via chemical adsorption.

Adsorption isotherms

Freundlich and Langmuir, as well as adsorption isotherm models, were utilized to standardize the adsorption results. Figure 7 shows the adsorption isotherms of SBA-15@BDA NPs for Pb^{2+} ions at equilibrium concentration. The Freundlich and Langmuir adsorption models were determined using the following equations (Santhamoorthy et al., 2023b). Table 2 shows the estimated Freundlich and Langmuir constants.

$$q_e = K_F + c_e^{1/2} \quad (5)$$

$$q_e = q_m K_L c_e / 1 + K_L c_e \quad (6)$$

where c_e: equilibrium concentration of adsorbate; q_e: adsorbed amount in the equilibrated solution; q_m (mg/g): theoretical maximum adsorption capacity; K_F (mg/g)(L/mg)(1/n): Freundlich constant; K_L (L/mg): Langmuir isotherm constant; n: adsorption intensity.

As shown in Table 2, the R^2 value for the Langmuir model (0.99) was close to 1 and larger than the R^2 value for the Freundlich model (0.99), indicating that the Langmuir plot had a good linear relationship (Table 2). The SBA-15@BDA NPs were found to have higher Pb^{2+} ion adsorption, with

Table 3 The adsorption capacity of the SBA-15@BDA NPs with the other adsorbent materials

Adsorbents	Adsorption capacity (mg/g)	References
For Pb^{2+} ions:		
Activated carbon	33.6	Zhang et al. (2016)
Alginate-chitosan composite	90.8	Kobya et al. (2005)
Fe_3O_4@APS@AA-co-CA MNPs	29.6	Hamza et al. (2021)
Poly (amide-hydrazide-imide)s containing L-aspartic acid	79.6	Ge et al. (2012)
HEMA-PGMA functionalized DETA	35.9	Vakili et al. (2015)
Functionalized Fe_3O_4@SiO_2@HA NPs	112	This work

values of ~ 112 mg/g. These suggest that the SBA-15@BDA NPs may be used for selective adsorption of Pb^{2+} ions from an aqueous solution.

Dose-dependent adsorption capacity

Using Pb^{2+} ion solutions with concentrations of 100 mg/L, at 25 °C, various adsorbent doses (0.025, 0.05, 0.75, 0.1, and 0.15 g), respectively, were used to assess the influence of adsorbent dose on the adsorption of Pb^{2+} ions on SBA-15@BDA NPs. With higher adsorbent dosage, the SBA-15@BDA NPs demonstrated improved metal ion adsorption efficiency, as seen in Fig. 8. With an adsorption amount of ~ 112 mg/g Pb^{2+} ions, the equilibrium adsorption capacity of Pb^{2+} ions was around ~ 86%. According to the study, the SBA-15@BDA NPs (0.1 g) may effectively adsorb up to ~ 86% of the Pb^{2+} ions from the initial metal ion solution (100 mg/L) at concentrations. Because surface functionalized amine groups, which are responsible for metal ion adsorption from aqueous solutions, are more abundant in SBA-15@BDA NPs, a higher adsorbent dose (0.15 g) led to increased Pb^{2+} ion adsorption.

Adsorption selectivity

The selective adsorption behavior of SBA-15@BDA NPs towards Pb^{2+} ions was determined in the presence of other competing heavy metal ions (Pb^{2+}, Ni^{2+}, Co^{2+}, Cd^{2+}, Zn^{2+} ions) and common metal ions (Na^{+}, K^{+}, Ca^{2+}, and Mg^{2+}) present in the initial solution. Figure 9 shows the SBA-15@BDA NPs displayed higher adsorption selectivity, and adsorption capacity (Fig. 9a, b) towards Pb^{2+} ions in an aqueous solution containing a mixture of heavy metal ions and common cations. In the initial solution containing common metal ions (Na^{+}, K^{+}, Ca^{2+}, and Mg^{2+}) and competing heavy metal ions (Pb^{2+}, Ni^{2+}, Co^{2+}, Cd^{2+}, and Zn^{2+}), the preferential adsorption behavior of SBA-15@BDA NPs towards Pb^{2+} ions was ascertained. Figure 9 illustrates that in an aqueous solution comprising a combination of heavy metal ions and common cations, the SBA-15@BDA NPs demonstrated better adsorption selectivity (Fig. 9a) and adsorption capacity (Fig. 9b) towards Pb^{2+} ions. However, the presence of additional interfering metal ions barely reduced their selectivity. These results verified that the selective adsorption of Pb^{2+} ions was not considerably hampered by the other competing metal ions (Mohan et al., 2024).

The amount of Pb^{2+} ions adsorption from the interfering metal ion solution was determined to be ~ 112 mg/g Pb^{2+} ions. However, as can be seen in Fig. 9b, the SBA-15@BDA NPs had a significantly lower adsorption capability than the other heavy metal ions that interfered. These results demonstrate that, in comparison to other metal ions, the amine functional groups in SBA-15@BDA NPs have a significantly higher complexation affinity towards Pb^{2+} ions. Because they formed a more stable combination with the Pb^{2+} ions, the SBA-15@BDA NPs demonstrated greater selectivity toward Pb^{2+} ions (Manoj et al., 2023).

Reusability study

The SBA-15@BDA NPs' reusability efficiency was assessed by subjecting the 0.1 g of SBA-15@BDA NPs adsorbent to solutions containing Pb^{2+} ions. The adsorbed metal ion was then leached out by treating the metal adsorbed samples with HCl solution (10 mL, 0.1 M), which was separated, rinsed with water, and neutralized with $NaHCO_3$ (0.1 M). Next, the metal ion adsorbed SBA-15@BDA NPs were isolated from the adsorption medium. In the following adsorption cycle, the sample of SBA-15@BDA NPs that had been regenerated was used. The effectiveness of SBA-15@BDA NPs' adsorption and desorption is shown in Fig. 10. SBA-15@BDA NPs demonstrated nearly five consecutive adsorption–desorption cycles, as shown in Fig. 10, without significantly decreasing Pb^{2+} ion adsorption capabilities. These findings indicate that the SBA-15@BDA NPs might be utilized as a reusable adsorbent for at least five consecutive adsorption processes (Table 3).

Conclusions

In conclusion, in this work, functionalized SBA-15@BDA NPs with amine groups were synthesized and their selective metal adsorption effectiveness was investigated. Instrumental techniques were used to characterize the prepared SBA-15@BDA

NPs. The study investigated the adsorption selectivity of SBA-15@BDA NPs under various conditions, such as solution pH, contact time, adsorbent dosage, and interfering metal ions. Even in the presence of other competitive metal ions, the SBA-15@BDA NPs demonstrated preferential adsorption efficiency towards ~ 86% Pb^{2+} ions, with maximum adsorption of ~ 112 mg/g Pb^{2+} ions at pH 6.5. Furthermore, the presence of other competing metal ions had no noticeable impact on the selective adsorption efficiency of SBA-15@BDA NPs. Additionally, the results of the pseudo-second-order kinetics investigation and the Langmuir isotherm show that the SBA-15@BDA NPs exhibit monolayer adsorption behavior. The findings of the adsorption–desorption process show that there is no significant reduction in adsorption efficiency when the SBA-15@BDA NPs is regenerated and reused up to five times. As a result, Pb^{2+} ions from aqueous solutions may be selectively adsorbed using the SBA-15@BDA NPs.

Acknowledgements This research was supported by the Basic Science Research Program through the National Research Foundation of Korea (NRF) funded by the Ministry of Education (2020R1I1A3052258). The authors express their sincere appreciation to the Researchers Supporting Project Number (RSP2024R466) King Saud University, Riyadh, Saudi Arabia

Author contributions K.T., M.S., R.S.: Conceptualization, methodology; M.A.W., M.C.L.: validation; K.T., S.C.M., M.S.: formal analysis; K.K., T.T.V.P.: resources, data curation; K.T., M.S.: writing—original draft preparation; R.S., M.A.W., M.C.L., S.C.K.: writing—review and editing, T.T.V.P., K.K.; visualization and supervision, All authors have read and agreed to the published version of the manuscript.

Data availability No datasets were generated or analysed during the current study.

Declarations

Conflict of interest The authors declare no competing interests.

References

Angon, P. B., Islam, M. S., Kc, S., Das, A., Anjum, N., Poudel, A., & Suchi, S. A. (2024). Sources, effects and present perspectives of heavy metals contamination: Soil, plants and human food chain. *Heliyon, 10*, e28357.

Ashbolt, N. J. (2004). Microbial contamination of drinking water and disease outcomes in developing regions. *Toxicology, 198*(1), 229–238.

Aziz, K. H. H., Mustafa, F. S., Omer, K. M., Hama, S., Hamarawf, R. F., & Rahman, K. O. (2023). Heavy metal pollution in the aquatic environment: Efficient and low-cost removal approaches to eliminate their toxicity: A review. *RSC Advances, 13*(26), 17595–17610.

Bharathiraja, S., Manivasagan, P., Moorthy, M. S., Bui, N. Q., Lee, K. D., & Oh, J. (2017). Chlorin e6 conjugated copper sulfide nanoparticles for photodynamic combined photothermal therapy. *Photodiagnosis and Photodynamic Therapy, 19*, 128–134.

Bharathiraja, S., Seo, H., Manivasagan, P., Moorthy, M. S., Park, S., & Oh, J. (2016). In vitro photodynamic effect of phycocyanin against breast cancer cells. *Molecules, 21*, 1470.

Bhasin, T., Lamture, Y., Kumar, M., & Dhamecha, R. (2023). Unveiling the health ramifications of Lead poisoning: A narrative review. *Cureus, 15*(10), e46727.

Briffa, J., Sinagra, E., & Blundell, R. (2020). Heavy metal pollution in the environment and their toxicological effects on humans. *Heliyon, 6*, e04691.

Collin, M., Venkataraman, S. K., Vijayakumar, N., Kanimozhi, V., Arbaaz, S. M., Stacey, R. G. S., Anusha, J., Choudhary, R., Lvov, V., Tovar, G. I., Koppala, S., & Swamiappan, S. (2022). Bioaccumulation of lead (Pb) and its effects on human: A review. *Journal of Hazardous Materials Advances, 7*, 100094.

Du Plessis, A. (2022). Persistent degradation: Global water quality challenges and required actions. *One Earth, 5*, 129–131.

Du, Y., Xue, X., Jiang, Q., Huang, W., Yang, H., Jiang, L., Jiang, B., & Komarneni, S. (2023). Ring-opening mechanism of epoxides with alcohol and tertiary amines. *Polymer Chemistry, 14*, 3679–3685.

Fu, F., & Wang, Q. (2011). Removal of heavy metal ions from wastewaters: A review. *Journal of Environmental Management, 92*, 407–418.

Ge, F., Li, M. M., Ye, H., & Zhao, B. X. (2012). Effective removal of heavy metal ions Cd^{2+}, Zn^{2+}, Pb^{2+}, Cu^{2+} from aqueous solution by polymer-modified magnetic nanoparticles. *Journal of Hazardous Materials, 212*, 366–372.

Hamza, M. F., Hamad, N. A., Hamad, D. M., Khalafalla, M. S., Abdel-rahman, A. A., Zeid, I. F., Wei, Y., Hessien, M. M., Fouda, A., & Salem, W. M. (2021). Synthesis of eco-friendly biopolymer, alginate-chitosan composite to adsorb the heavy metals, Cd(II) and Pb(II) from contaminated effluents. *Materials, 14*, 2189.

Harikrishnan, T., Sivakumar, P., Sivakumar, S., Arumugam, S., Raman, T., Singaram, G., Thangavelu, M., Kim, W., & Muthusamy, G. (2024). Effect of microfibers induced toxicity in marine sedentary polychaete *Hydroides elegans*: Insight from embryogenesis axis. *Science of the Total Environment, 906*, 167579.

Kobya, M., Demirbas, E., Senturk, E., & Ince, M. (2005). Adsorption of heavy metal ions from aqueous solutions by activated carbon prepared from apricot stone. *Bioresource Technology, 96*, 1518–1521.

Kumar, M., Shekhar, S., Kumar, R., Kumar, P., Govarthanan, M., & Chaminda, T. (2023). Drinking water treatment

and associated toxic byproducts: Concurrence and urgence. *Environmental Pollution, 320*, 121009.

Liosis, C., Papadopoulou, A., Karvelas, E., Karakasidis, T. E., & Sarris, I. E. (2021). Heavy metal adsorption using magnetic nanoparticles for water purification: A critical review. *Materials, 14*(24), 7500.

Liu, H., Fu, T., & Mao, Y. (2022). Metal–organic framework-based materials for adsorption and detection of uranium(VI) from aqueous solution. *ACS Omega, 7*(17), 14430–14456.

Manivasagan, P., Bharathiraja, S., Moorthy, M. S., Oh, Y.-O., Song, K., Seo, H., & Oh, J. (2017a). Anti-EGFR antibody conjugation of fucoidan-coated gold nanorods as novel photothermal ablation agents for cancer therapy. *ACS Applied Materials & Interfaces, 9*, 14633–14646.

Manivasagan, P., Bui, N. Q., Bharathiraja, S., Moorthy, M. S., Oh, Y., Song, K., Seo, H., Yoon, M., & Oh, J. (2017b). Multifunctional biocompatible chitosan-polypyrrole nanocomposites as novel agents for photoacoustic imaging-guided photothermal ablation of cancer. *Science and Reports, 7*, 43593.

Manoj, D., Rajendran, S., Naushad, M., Santhamoorthy, M., Gracia, F., Moscoso, M. S., & Gracia-Pinilla, M. A. (2023). Mesoporogen free synthesis of CuO/TiO_2 heterojunction for ultra-trace detection of catechol in water samples. *Environmental Research, 216*, 114428.

Mitra, S., Chakraborty, A. J., Tareq, A. M., Emran, T. B., Nainu, F., Khusro, A., Idris, A. M., Khandaker, M. U., Osman, H., Alhumaydhi, F. A., & Simal-Gandara, J. (2022). Impact of heavy metals on the environment and human health: Novel therapeutic insights to counter the toxicity. *Journal of King Saud University - Science, 34*, 101865.

Mohan, A., Suresh, R., Ashwini, M., Periyasami, G., Guganathan, L., Lin, M.-C., Kumarasamy, K., Kim, S. C., & Santhamoorthy, M. (2024). Alginate functionalized magnetic-silica composites for pH-responsive drug delivery and magnetic hyperthermia applications. *Materials Letters, 361*, 136088.

Moorthy, M. S., Bae, J. H., Kim, S. H., & Ha, C. S. (2013e). Design of a novel mesoporous organosilica hybrid microcarrier: A pH stimuli-responsive dual-drug-delivery vehicle for intracellular delivery of anticancer agents. *Particle & Particle Systems Characterization, 30*, 1044–1055.

Moorthy, M. S., Bharathiraja, S., Manivasagan, P., Lee, K. D., & Oh, J. (2017a). Crown ether triad modified core–shell magnetic mesoporous silica nanocarrier for pH-responsive drug delivery and magnetic hyperthermia applications. *New Journal of Chemistry, 41*, 10935–10947.

Moorthy, M. S., Bharathiraja, S., Manivasagan, P., Lee, K. D., & Oh, J. (2017b). Synthesis of surface capped mesoporous silica nanoparticles for pH-stimuli responsive drug delivery applications. *MedChemComm, 8*, 1797–1805.

Moorthy, M. S., Bharathiraja, S., Manivasagan, P., Oh, Y., Phan, T. T. V., Mondal, S., Kim, H., Lee, K. D., & Oh, J. (2018). Synthesis of Fe_3O_4 modified mesoporous silica hybrid for pH-responsive drug delivery and magnetic hyperthermia applications. *Journal of Porous Materials, 25*, 1251–1264.

Moorthy, M. S., Cho, H. J., Yu, E. J., Jung, Y. S., & Ha, C. S. (2013a). A modified mesoporous silica optical nanosensor for selective monitoring of multiple analytes in water. *Chemical Communications, 49*, 8758–8760.

Moorthy, M. S., Kim, H. B., Bae, J. H., Kim, S. H., & Ha, C. S. (2016b). Design of core–shell magnetic mesoporous silica hybrids for pH and UV light stimuli-responsive cargo release. *RSC Advances, 35*, 29106–29115.

Moorthy, M. S., Kim, M. J., Bae, J. H., Park, S. S., Saravanan, N., Kim, S. H., & Ha, C. S. (2013b). Multifunctional periodic mesoporous organosilicas for biomolecule recognition, biomedical applications in cancer therapy, and metal adsorption. *European Journal of Inorganic Chemistry, 2013*, 3028–3028.

Moorthy, M. S., Oh, Y., Bharathiraja, S., Manivasagan, P., Rajarathinam, T., Jang, B., Phan, T. T. V., Jang, H., & Oh, J. (2016a). Synthesis of amine-polyglycidol functionalised $Fe_3O_4@SiO_2$ nanocomposites for magnetic hyperthermia, pH-responsive drug delivery, and bioimaging applications. *RSC Advances, 6*, 110444–110453.

Moorthy, M. S., Park, S. S., Mathew, A., Lee, S. H., Lee, W. K., & Ha, C. S. (2014b). Amidoxime functionalized SBA-15 for selective adsorption of Li+ ions. *Science of Advanced Materials, 6*, 1611–1617.

Moorthy, M. S., Seo, D. J., Song, H. J., Park, S. S., & Ha, C. (2013f). Magnetic mesoporous silica hybrid nanoparticles for highly selective boron adsorption. *Journal of Materials Chemistry A, 1*, 12485–12496.

Moorthy, M. S., Song, H. J., Bae, J. H., Kim, S. H., & Ha, C. S. (2014a). Red fluorescent hybrid mesoporous organosilicas for simultaneous cell imaging and anticancer drug delivery. *RSC Advances, 4*, 43342–43345.

Moorthy, M. S., Tapaswi, P. K., Park, S. S., Mathew, A., Cho, H. J., & Ha, C. S. (2013c). Ion-imprinted mesoporous silica hybrids for selective recognition of target metal ions. *Microporous and Mesoporous Materials, 180*, 162–171.

Nagappan, S., Choi, M. C., Sung, G., Park, S. S., Moorthy, M. S., Chu, S. W., Lee, W. K., & Ha, C. S. (2013). Highly transparent, hydrophobic fluorinated polymethylsiloxane/silica organic-inorganic hybrids for anti-stain coating. *Macromolecular Research, 21*, 669–680.

Oh, Y., Moorthy, M. S., Manivasagan, P., Bharathiraja, S., & Oh, J. (2017). Magnetic hyperthermia and pH-responsive effective drug delivery to the sub-cellular level of human breast cancer cells by modified $CoFe_2O_4$ nanoparticles. *Biochimie, 133*, 7–17.

Parambadath, S., Rana, V. K., Moorthy, S., Chu, S. W., Park, S. K., Lee, D., Sung, G., & Ha, C. S. (2011). Periodic mesoporous organosilicas with co-existence of diurea and sulfanilamide as an effective drug delivery carrier. *Journal of Solid State Chemistry, 184*, 1208–1215.

Park, S. S., Moorthy, M. S., Song, H. J., & Ha, C. S. (2014). Functionalized mesoporous silicas with crown ether moieties for selective adsorption of lithium ions in artificial sea water. *Journal of Nanoscience and Nanotechnology, 14*, 8845–8851.

Petrovic, B., Gorbounov, M., & Soltani, S. M. (2022). Impact of surface functional groups and their introduction methods on the mechanisms of CO_2 adsorption on porous

carbonaceous adsorbents. *Carbon Capture Science & Technology, 3*, 100045.

Phan, T. T. V., Moorthy, M. S., Kang, H. W., Nam, S. Y., Lee, Y. W., & Oh,. (2018). Coating chitosan thin shells: A facile technique to improve dispersion stability of magnetoliposomes. *Journal of Nanoscience and Nanotechnology, 18*, 583–590.

Raj, K., & Das, A. P. (2023). Lead pollution: Impact on environment and human health and approach for a sustainable solution. *Environmental Chemistry and Ecotoxicology, 5*, 79–85.

Reddy, C. P. K., Manikandavelu, D., Arisekar, U., Ahilan, B., Uma, A., Jayakumar, N., Kim, W., Govarthanan, M., Harini, C., Vidya, R. S., Madhavan, N., & Reddy, D. R. K. (2023). Toxicological effect of endocrine disrupting insecticide (deltamethrin) on enzymatical, haematological and histopathological changes in the freshwater iridescent shark, *Pangasius hypothalamus*. *Environmental Toxicology and Pharmacology, 101*, 104201.

Santhamoorthy, M., Thirumalai, D., Thirupathi, K., & Kim, S. C. (2023b). Synthesis of dithiol-modified mesoporous silica adsorbent for selective adsorption of mercury ions from wastewater. *Applied Nanoscience, 13*, 6015–6024.

Santhamoorthy, M., Thirupathi, K., Krishnan, S., Guganathan, L., Dave, S., Phan, T. T. V., & Kim, S.-C. (2023a). Preparation of magnetic iron oxide incorporated mesoporous silica hybrid composites for pH and temperature-sensitive drug delivery. *Magnetochemistry, 9*(3), 81.

Santhamoorthy, M., Thirupathi, K., Thirumalai, D., Aldawood, S., & Kim, S. C. (2022). Surface grafted silica adsorbent for efficient removal of Hg^{2+} ions from contaminated water. *Environmental Research, 212*, 113211.

Singh, V., Ahmed, G., Vedika, S., Kumar, P. S., Chaturvedi, S. K., Nand, S., Vamanu, E., & Kumar, A. (2024). Toxic heavy metal ions contamination in water and their sustainable reduction by eco-friendly methods: Isotherms, thermodynamics and kinetics study. *Science and Reports, 14*, 7595.

Tahreen, A., Jami, M. S., & Ali, F. (2020). Role of electrocoagulation in wastewater treatment: A developmental review. *Journal of Water Process Engineering, 37*, 101440.

Taslima, K., Al-Emran, M., Rahman, S., Hasan, J., Ferdous, Z., Rohani, M. F., & Shahjahan, M. (2022). Impacts of heavy metals on early development, growth and reproduction of fish—A review. *Toxicology Reports., 9*, 858–863.

Thirupathi, K., Phan, T. T. V., Santhamoorthy, M., Ramkumar, V., & Kim, S. C. (2022). pH and Thermoresponsive PNIPAm-co-polyacrylamide hydrogel for dual stimuli-responsive controlled drug delivery. *Polymers, 15*, 167.

Thirupathi, K., Rajesh, S., Madhappan, S., Gnanasekaran, L., Guganathan, L., Phan, T. T. V., & Kim, S. C. (2023). Selective removal of copper(II) ions from aqueous solution using pyridyl-bridged mesoporous organosilica hybrid adsorbent. *Environmental Research, 224*, 115439.

Vakili, M. R., Zahmatkesh, S., Panahiyan, M. J., & Jafarizadeh, T. (2015). Poly(amide-hydrazide-imide)s containing L-aspartic acid: synthesis, characterization, and their applications in removal of heavy metal ions. *Designed Monomers and Polymers, 18*, 315–322.

Venugopal, V., Balaji, D., Preeyanghaa, M., Moon, C. J., Neppolian, B., Muthusamy, G., Theerthagiri, J., Madhavan, J., & Choi, M. Y. (2023). Synergistic combination of $BiFeO_3$ nanorods and $CeVO_4$ nanoparticles for enhanced visible light driven photocatalytic activity. *Alexandria Engineering Journal, 72*, 531.

Zhang, N., Zang, G. L., Shi, C., Yu, H. Q., & Sheng, G. P. (2016). A novel adsorbent TEMPO-mediated oxidized cellulose nanofibrils modified with PEI: Preparation, characterization, and application for Cu(II) removal. *Journal of Hazardous Materials, 316*, 11–18.

Zhang, P., Yang, M., Lan, J., Huang, Y., Zhang, Y., Huang, S., Yang, Y., & Ru, J. (2023). Water quality degradation due to heavy metal contamination: Health impacts and eco-friendly approaches for heavy metal remediation. *Toxics, 11*(10), 828.